

Reverse pulse strategies for silicon dioxide thin films deposition by high power impulse magnetron sputtering.

ONISZCZUK, AW, OWEN, David, LOCH, DAL, HOVSEPIAN, Papken
<<http://orcid.org/0000-0002-1047-0407>> and EHIASARIAN, Arutiun
<<http://orcid.org/0000-0001-6080-3946>>

Available from Sheffield Hallam University Research Archive (SHURA) at:

<https://shura.shu.ac.uk/35434/>

This document is the Published Version [VoR]

Citation:

ONISZCZUK, AW, OWEN, David, LOCH, DAL, HOVSEPIAN, Papken and EHIASARIAN, Arutiun (2025). Reverse pulse strategies for silicon dioxide thin films deposition by high power impulse magnetron sputtering. *Surface and Coatings Technology*, 505: 132117. [Article]

Copyright and re-use policy

See <http://shura.shu.ac.uk/information.html>



Reverse pulse strategies for silicon dioxide thin films deposition by high power impulse magnetron sputtering[☆]

A.W. Oniszczyk^a, D.S. Owen^b, D.A.L. Loch^c, P.Eh. Hovsepian^d, A.P. Ehiasarian^{d,*}

^a Trumpf Huettinger Sp. z o.o., Zielonka, Poland

^b Biomolecular Sciences Research Centre, Sheffield Hallam University, Howard St., Sheffield S1 1WB, UK

^c Trumpf Hüttinger GmbH + Co. KG, Freiburg, Germany

^d National HIPIMS Technology Centre – UK, Sheffield Hallam University, Howard St., Sheffield S1 1WB, UK

ARTICLE INFO

Keywords:

High power impulse magnetron sputtering
Silicon dioxide
Plasma characterisation
Dielectric materials

ABSTRACT

High density transparent oxide layers on polymers and glass can improve the environmental viability of photovoltaics, displays, and low emissivity layers in glazing as well as aid the design of optical filters. High Power Impulse Magnetron Sputtering (HIPIMS) produces high density microstructures and high hardness due to the delivery of an ionised metal and dissociated Oxygen deposition flux to the substrates. Silicon dioxide (SiO₂) films were deposited by reactive HIPIMS of a metallic target in an Argon-Oxygen atmosphere. Single-target HIPIMS sputtering with reverse voltage operation was evaluated. The HIPIMS process was carried out by controlling the current within the pulse. This resulted in the elimination of stability issues associated with runaway currents for all target poisoning states from metallic to compound. SiO₂ was deposited at a peak current density of 0.5 Acm⁻² in a plasma dominated by Si¹⁺ ions as shown by energy- and mass- resolved spectrometry. The measured signal of atomic Oxygen was twice the amount of molecular Oxygen. The pulse duration was 20 microseconds. Plasma persisted to >150 μs after the pulse switch off as evidenced by the Ar neutral (Ar I) optical emission intensity. Arcing rates were significantly reduced when reverse pulsing was used due to the discharging of the target surface. The key attributes of the reverse voltage which influenced the extent of film defects caused by arcing events and deposition conditions were the amplitude and the delay between the switch-off of the pulse and the application of the reverse voltage. Applying a reverse voltage immediately after the end of the pulse utilised the undispersed high-density plasma still present in the racetrack at the point of switch off to neutralise the target surface and reduce arc energy. Reverse voltages of +25 V coupled with short delay times resulted in enhancing the flux and augmenting the energy of metal ions to the substrate. The gains in adatom mobility afforded by this approach promoted the formation of smooth and dense films with microscopic roughness of R_a = 3 nm as observed by AFM and high optical transmittivity of up to 97 % at a wavelength of 800 nm for 200 nm thick films. The high density supported a high nanohardness of 1 μm thick films of 10 ± 1 GPa and Young's modulus 77 ± 9 GPa, representing a 10 % increase over a glass substrate. Reverse voltages of +75 V and beyond were detrimental due to the production of ions of process and contaminant gases near the chamber walls and the target, which disrupted the lateral growth of film grains and induced the formation of globular morphology with a high microscopic surface roughness.

1. Introduction

Silicon dioxide thin films are in demand for environmental and mechanical protection of photovoltaic cells [1,2], electronic displays [1], dielectric layers in microelectronic components [3], anti-reflection optical coatings [4] and low-index layers in optical filter stacks for

architectural glazing [4]. All of these applications can benefit from improving the density of the films, however, standard deposition techniques such as magnetron sputtering produce globular microstructures [5] due to the low energy of the depositing atoms and incorporation of impurities [6]. High power impulse magnetron sputtering (HIPIMS) technology utilises high power density glow discharges to produce

[☆] This article is part of a Special issue entitled: 'Multifunctional Coatings' published in Surface & Coatings Technology.

* Corresponding author.

E-mail address: a.ehiasarian@shu.ac.uk (A.P. Ehiasarian).

<https://doi.org/10.1016/j.surfcoat.2025.132117>

Received 17 December 2024; Received in revised form 19 March 2025; Accepted 31 March 2025

Available online 1 April 2025

0257-8972/© 2025 The Authors. Published by Elsevier B.V. This is an open access article under the CC BY license (<http://creativecommons.org/licenses/by/4.0/>).

plasma densities that reach a critical level beyond which significant ionisation of the sputtered flux is enabled [7,8].

A major challenge in synthesising SiO_x films in a plasma glow discharge environment is the high probability of transitioning to an arc discharge that produces macroparticles which are embedded in the film and create large-scale morphological defects due to shadowing of the deposition flux. There are two main causes for arcing events. The surface of the target contains microscopic asperities which are bombarded by the high density plasma fluxes and, at specific locations, may reach temperatures sufficient to induce thermoelectron emission [9,10]. Once initiated, electron emission develops to high current densities within the asperities converting them to a state that can be characterised either as a high-density plasma or superhot solid. Meanwhile, the material adjacent to the asperities melts. The particles within the asperity experience enormous pressure which results in an explosion and launching of vapour phase whilst also acting on the molten material and causing ejection in the form of macroparticles (droplets). The critical current required for an asperity to sublime scales with the density and the inverse of the electrical and thermal conductivity of the material. The discharge transitions from glow to arc with the plasma contracting to a few micrometres area and the voltage dropping to tens of volts.

Additionally, in insulating materials - such as the SiO_x compound layer formed during sputtering in reactive atmosphere - the interaction of the plasma with the target results in an accumulation of ion charge onto the surface. When the charge reaches a critical level, an insulator breakdown occurs, resulting in local heating and melting as well as macroparticle generation. Reversing the voltage on the target periodically, discharges the surface and helps to reduce arcing [11] – the so-called “reverse voltage” operation. In systems with two (dual) magnetrons, a similar effect can be achieved through the “bipolar” operation, whereby one of the magnetrons plays the role of a cathode and the other an anode and their roles are reversed in consecutive pulses. In single-magnetron systems, HIPIMS with reverse voltage operation is implemented whereby the positive pulses on the target are applied with a short delay after the main negative discharge pulse is completed. Typically the delay is chosen so that the reverse voltage is applied while there is an afterglow plasma with a high density and which has established a sheath both around the walls which are electrically grounded and the substrates which can be either electrically insulated (floating) or negatively biased [12]. The effect of the positive target potential is to raise the plasma potential above it and accelerate electrons across the potential of sheaths formed at all other surfaces such as the grounded walls which are negatively charged with respect to the bulk plasma. While traversing the sheath the electrons can gain energies above 20 eV, which are sufficient to ionise the gas in the vicinity [13], with the highest efficiency achieved when the voltage approaches the range 70–100 V, where the ionisation cross section for most inert gases is near its maximum. The long off-time between HIPIMS pulses provides sufficient time for positive pulses to ignite an auxiliary plasma near the walls and substrates and very long positive pulses can give rise to fireballs [13]. The production of process gas ions is augmented during the positive voltage phase [14].

Silicon dioxide is a challenging material to synthesise as it combines poor electrical and thermal conductivity with highly insulating properties, thus the deposition of such thin films in a plasma environment is often unstable, leading to high probability of glow-to-arc transition events on the target. Particularly in magnetron sputtering from a Si target in oxygen atmosphere, a SiO_x compound tends to cover the target and dominate the behaviour of the system. Therefore, typical plasma synthesis processes are limited to low power, producing porous microstructure and rough surfaces. Meanwhile, great benefits can be gained by densifying the microstructure in terms of lower surface roughness, better wear resistance and better electrical and optical performance. The hardness of SiO_x films has been linked to the abrasion resistance against sand [15]. Depending on the deposition process, a significant variation of hardness values is obtained. Low-energy deposition environments

such as plasma-assisted chemical vapour deposition (PACVD) produce a hardness of 0.5–2.3 GPa depending on the degree of polymerisation [2]. More energetic processes can increase the hardness to 4.1 GPa for hollow cathode plasma activated electron beam evaporation [5], and 8 GPa for pulsed DC magnetron sputtering [5,15]. Hardness of up to 9.8 GPa has been reported for TiO₂/SiO₂ optical filter multi-layer stacks produced by microwave-assisted magnetron sputtering [16].

In this work we explore the deposition of highly insulating Silicon Dioxide films using HIPIMS, aiming at raising the adatom mobility of the deposition flux through maximizing the rates of Si ion production, whilst obtaining a stable process where arcing-induced damage to the films minimised. To achieve this, HIPIMS is driven with a reverse voltage applied after the main negative pulse. Different modes of voltage reversal including a variety of amplitudes and delays after the negative pulse shut-off are analysed. Ion flux composition, discharge development and film morphology, optical transmittance and nano-hardness are analysed. We expect these strategies to be applicable to the synthesis of a wide range of insulating materials.

2. Experimental details

Plasma analyses and thin film synthesis were carried out in a CMS 18 sputtering system (Kurt J Lesker Ltd., UK) equipped with a 3-inch unbalanced magnetron (Fig. 1). The substrates were mounted at a distance of 120 mm from the target and were rotated at a speed of 5 rpm. The base pressure was in the range $4\text{--}8 \times 10^{-7}$ mbar. The samples were not heated intentionally and the temperature was 19 °C. During deposition, the total pressure was 1.9×10^{-3} mbar and Ar flow was 20 sccm and O₂ flow was 7 sccm. The cathode voltage was set to $U_d = -800$ V. The arc detection circuit was set to a maximum current thresholds of $I_{\max} = 50$ A. A parallel “arc cross-detection” circuit monitored simultaneously the voltage and current with thresholds for voltage of below $U_x = -600$ V and current above $I_x = 35$ A.

A HIPIMS generator TruPlasma Highpulse 4002 G2 (TRUMPF Huettinger Sp. z o.o., Poland) was used to control the discharge current. The generator applies power in two stages – initially, during an ignition stage, the voltage is kept constant over a duration which is just long enough to ignite the discharge. This stage is followed by a longer, current-controlled stage. Typically, the ignition stage operates at high voltages (near –2 kV) to achieve a fast rise of the discharge current and

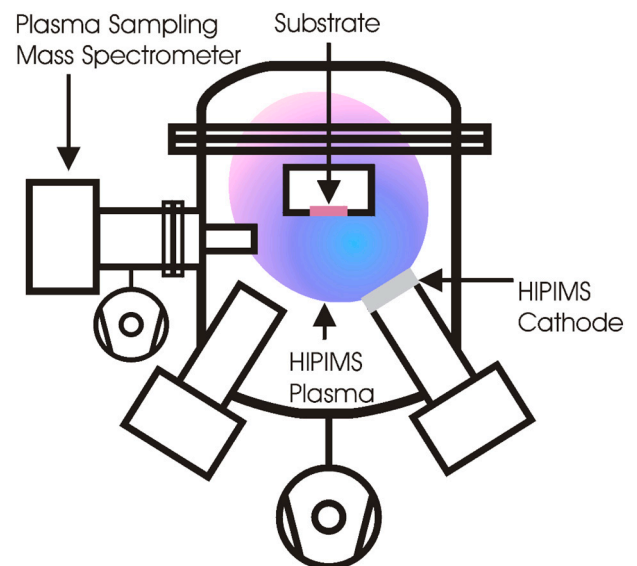


Fig. 1. Schematic cross section of the deposition system showing the positions of the cathode, substrate, and mass spectrometer. The HIPIMS cathode was furnished with a Si target.

ignition of the discharge. However, in the case of SiO_x, which is highly insulating, such approach led to excessive arcing. Therefore, these experiments aimed at achieving a slow rate of rise in the current, in a controlled and reproducible fashion. To achieve this goal, the experiments were carried out using the ignition stage only, where the voltage level was kept low (−1350 V) and constant throughout the pulse. The pulse current was regulated by the applied voltage and impedance of the circuit to achieve an exponential increase. The peak current was set to 24 A, the pulse duration was set to 20 μs and pulse frequency was 500 Hz. The internal cable length compensation (CLC) circuit was employed to apply a positive voltage on the target within 500 ns of the end of the negative pulse, producing a double pulse of amplitude +120 V and duration of 1 μs for each pulse, as shown in the waveform in Fig. 2a. CLC is a quick-acting feature that accelerates the shut off of energy delivery to the target at the end of the pulse by redirecting the energy stored in the cables away from the target and into the generator (patented by TRUMPF Huettinger). In order to rapidly cut off current delivery, the polarization of the power supply output is reversed. In contrast to standard voltage reversal, where the level is set by the operator, CLC derives its reverse voltage from the current flowing through the cables at the time of switch-off. The reverse voltage in CLC depends on the “current lag” with respect to the voltage and persists until the current goes to zero (no more energy in cables). In normal operation, the CLC reverse voltage is not detectable on the target. As CLC was calibrated for currents up to 2 kA, it was not accurate at the low currents (24 A) used in the experiments described here and resulted in a positive voltage arising at the target. The inbuilt positive-pulsing unit was also deployed with programmable delay in the range 0.001–20.000 μs and amplitude 0–150 V. The voltage was measured using a differential voltage probe type TA044 (Pico Technology Ltd., UK) with an attenuation factor of 1000:1 and frequency bandwidth of 70 MHz. The current was measured using a Rogowski coil type CWT15 (Power Electronic Measurements Ltd., UK). A DPO7504 oscilloscope was used to record the current and voltage waveforms over 512 averages.

An energy-resolved mass spectrometer model PSM003 (Hiden Analytical Ltd., UK) with a grounded particle-sampling orifice was used to collect ion energy distribution functions in time-averaged mode. The relative flux of ions was obtained by integrating the IEDF and calculating its relative fraction with respect to the sum of all IEDFs. For Silicon, both isotopes at 28 amu/e and 29 amu/e were measured and confirmed to be of ratio 92.18:4.71 to avoid confusion with common contaminants such as Nitrogen molecules. The efficiency of transmission and detection of ions in the mass spectrometer is known to reduce with mass-to-charge ratio through an unknown relation. Therefore, the absolute ion concentrations could not be obtained with sufficient accuracy without underestimating the heavier species. It is assumed that species with

similar mass-to-charge ratio such as Si¹⁺ (28) and Ar¹⁺ (40) are close enough to neglect differences in detection efficiency. Plasma emission was collected in vacuo through quartz fibre optic cable and a collimator directed at the dense plasma region (racetrack) of the magnetron. Optical emission spectra (OES) were obtained with a FHR1000 (Horiba Jobin Yvon, France) monochromator with a focal length of 1 m and resolution of 0.012 nm. Time-averaged spectra were collected with a Synapse CCD detector. Time-resolved optical emission intensities for Ar I and O I were collected with a time step of 0.3 ns using a photomultiplier detector type R955 (Hamamatsu) whose output was shunted to ground via a 300 kΩ resistor and fed via a 5 m long coaxial cable to a DPO7504 (Tektronix Inc., USA) oscilloscope with an input capacitance of 13 pF and input impedance of 1 MΩ. According to LTSpice simulations, the circuit responded to transient signals (pulses) with weak (1 mV) oscillations which were damped over 15 microseconds, which affected weaker OES signals such as O I. Signals were averaged over 512 measurements. A quartz crystal microbalance SQM-160 (Inficon) was used to monitor deposition rates.

The substrates were soda lime glass of thickness 1 mm. Prior to deposition, the substrates were cleaned in a sequence of ultrasonic baths of methylated spirit, acetone and deionised water.

The light transmission characteristics of the films were analysed using a UV-Vis spectrophotometer Varian Cary 50 (Varian Inc., USA). The film surface was imaged using an atomic force microscope type MultiMode 8-HR (Bruker) in contact mode and DNP-S10 tips with nominal radius of 10 nm and maximum radius of 40 nm. AFM data were analysed using NanoScope Analysis (Bruker Corporation) v. 1.50 (Build R2Sr2.111746). Statistical data were analysed using Prism (GraphPad Software Inc.) v 8.1.1 (330) for Windows. The instrumental hardness and elastic modulus were determined by nanoindentation (CSM, Switzerland) on 1 μm thick films using a load of 3 mN to achieve a penetration depth of 108 ± 3 nm.

The response of plasma parameters and coating properties to reverse pulse attributes of delay with respect to voltage switch-off (t_d), amplitude (U_r) and duration (t_r) was studied with the aid of a Box-Behnken design of experiment. For the plasma parameter measurements by energy-resolved mass spectroscopy, three levels were used for each reverse pulse attribute: $t_d = \{0, 10, 20\}$ μs, $U_r = \{+25, +75, +150\}$ V, and $t_r = \{0, 10, 20\}$ μs. For the coating parameters including macroscopic roughness, microscopic roughness and transmittivity, two or three levels were used: $t_d = \{0, 10\}$ μs, $U_r = \{+25, +150\}$ V, and $t_r = \{10, 20, 30\}$ μs. Response surfaces were calculated in MATLAB using linear regression fitting of a quadratic polynomial utilising the three reverse pulse attributes.

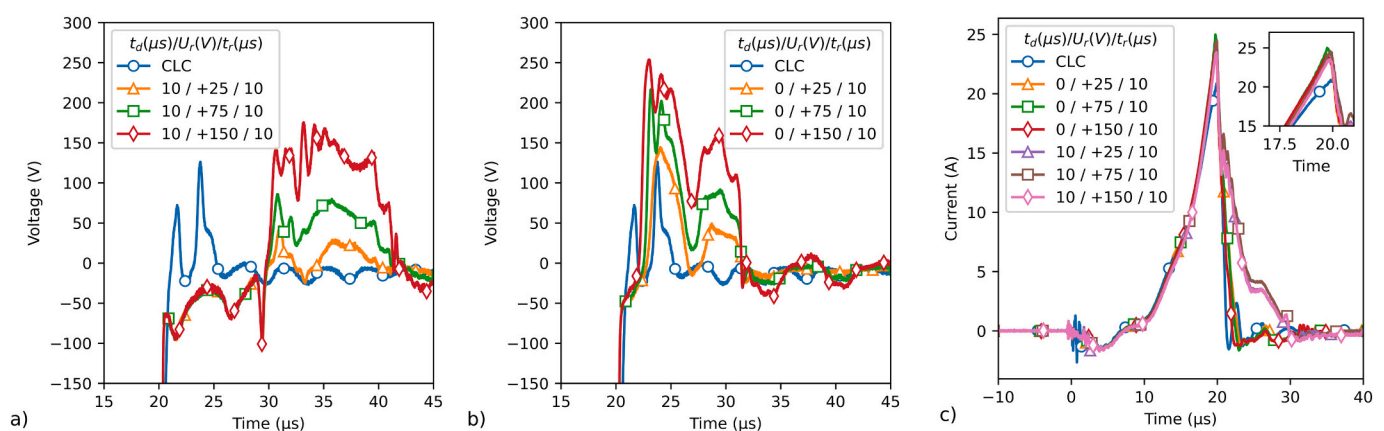


Fig. 2. Waveforms for reverse portion of the voltage measured at the cathode with CLC and amplitudes of $U_r = +25, +75,$ and $+150$ V applied with (a) delay of $t_d = 10$ μs and (b) no delay, and (c) waveforms for the discharge current including both the negative and positive voltage stages. Negative voltage is applied at $t = 0$ μs for a duration of 20 μs.

3. Results

3.1. Current-voltage characteristics

The reverse portion of the voltage and the complete current waveforms for seven representative pulse types are shown in Fig. 2a, b and c. In all cases, the negative portion of the pulse comprised a steady voltage without oscillations or droop and lasted from 0 to 20 μs . When no reverse voltage was applied (not shown), the potential at the cathode reduces quickly down to -100 V and then relaxes towards zero over the next 25 μs until 45 μs , staying negative throughout. Fig. 2a focuses on the reverse portion of the voltage waveform showing the time span from just before the end of the negative pulse at 15 μs until after the reverse voltage has been switched off at 45 μs . When CLC is activated, the voltage on the cathode reverses very rapidly changing from -800 V to $+72\text{ V}$ over 1.5 μs before falling back to 0 V. The CLC circuit then produces a second peak rising to $+128\text{ V}$. The two peaks together amount to a total reverse time of $\sim 2\text{ }\mu\text{s}$. The reverse voltage finally settles to 0 V at 25 μs . When the reverse circuit is activated without delay (Fig. 2b), the voltage falls rapidly to -50 V and gradually shifts to $+250\text{ V}$ over 3 μs , settling finally to 0 V at 32 μs , giving a total reverse time of 9 μs . The reverse circuit applies a positive voltage with an effective delay of 1.5 μs compared to the CLC circuit, which is double that of the CLC circuit. This is significant in the context of the rapid decay timescales observed for the discharge current as follows.

Fig. 2c shows the cathode current waveforms over both the negative and positive voltage stages corresponding to the seven pulse types shown in Fig. 2a and b. The peak current of 24 A (current density of 0.5 A cm^{-2}) is one order of magnitude higher than for conventional DC sputtering, indicating one order of magnitude greater plasma density in the target vicinity. The rise of the current is closely matched for all pulse types and comprises an exponential rise between 5 and 20 μs , confirming that the current shape is controlled reproducibly. The CLC circuit reaches slightly lower peak value than all other circuits as shown in the inset of Fig. 2c. The main differences are observed after the pulse-off point. When no reverse voltage was applied (not shown), the current decayed slowly reaching 0 A at 30 μs , giving a total decay time of 10 μs . When CLC is activated, the current drops rapidly with a decay time of $\sim 1.5\text{ }\mu\text{s}$, and is seen to reverse direction, reaching negative levels over approximately 5 μs , after which it settles to 0 A. With the reverse circuit activated without a delay, the decay time is $\sim 2.2\text{ }\mu\text{s}$. It is worth noting that the reverse circuit has an intrinsic delay which means that it applies its voltage with a 3 μs delay, when the current has decayed by $>99\%$. In contrast, the CLC circuit reaches positive voltages with delay of 1.5 μs where the current decay is 50%. The observed rapid reversal in current is consistent with reports on HIPIMS in inert gas environments [17].

The current is seen to dip to negative values at around 3 microseconds into the pulse. This is caused by oscillations which appeared when the voltage was applied even when a plasma was not ignited, and are therefore an artefact caused by stray capacitance and inductance in the cable connecting the power generator to the cathode. Overall, the voltage traces are a juxtaposition of the driven voltage and electrical

ringing. Due to the fast time scales of operation, the ringing occurs at similar time scales as the pulse duration.

3.2. Influential parameters determined from Box-Behnken analysis

To guide the detailed presentation of experimental results in the following sections, we determined the strongest dependencies between the set process parameters and experimentally obtained results on plasma chemistry and film properties by fitting response surfaces to results obtained from a Box-Behnken design-of-experiment matrix. Table 1 summarises the most influential parameters as determined from this analysis for selected ion flux ratios ($\text{Si}^{1+}:\text{Ar}^{1+}$, $\text{O}^{1+}:\text{O}_2^+$, $\text{Si}^{2+}:\text{Si}^{1+}$) and film properties including transmittance at 550 nm, macroscopic roughness Ra and microscopic roughness Ra.

The delay in applying the reverse pulse, t_d , was the parameter of primary or secondary importance across all features of interest. The reverse voltage amplitude, U_r , is the most influential parameter for the $\text{O}^{1+}:\text{O}_2^+$ ion flux ratio. The reverse pulse duration, t_r , was the principal component for microscopic roughness and the $\text{Si}^{2+}:\text{Si}^{1+}$ ion flux ratio and second-most influential for transmittance, and macroscopic roughness.

The analyses identified the reverse voltage delay and amplitude as the most influential parameters. They were used in subsequent analyses to determine the detailed relationship between process parameters and the plasma chemistry in Section 3.3, thin film morphology in Section 3.4, optical properties in Section 2.4 and nanohardness in Section 3.6. Focussing on the strongest dependencies allowed us to derive physical explanations of the underlying processes in Section 4.

3.3. Plasma chemistry – OES and mass spectrometry

Fig. 3a shows a spectrum of HIPIMS of Si plasma obtained in time-averaged mode. Emission from Si ions (Si II) at 784 nm and the atomic Oxygen (O I) triplet at 777.194, 777.4166 and 777.5388 nm are clearly visible along with the Ar neutral (Ar I) lines at 763.5 nm, 772 nm and 782 nm. Atomic oxygen is created via two important pathways – the dissociation of oxygen molecules via electron collisions and sputtering from the target. The former process occurs during both the negative and positive portions of the pulse, where energetic electrons are observed. As such it is sensitive to the parameters of the reverse positive voltage. In contrast, the latter process occurs only during the negative pulse stage when high negative voltages are present at the target surface.

The presence of Si ion emission is indicative of high plasma density as a result of the 10-fold increase in current (Fig. 2b). The time evolution of O I emission for different delays applied with the reverse circuit is shown in Fig. 3b. All pulse types exhibit a similar exponential rise during the on-time. An exponential decay is observed as well. However, when the reverse circuit is applied with a 10 and 20 μs delay, the emission is enhanced. The curve for O I emission with CLC circuit has been omitted as it is of too low intensity and the poor signal-to-noise ratio makes it difficult to interpret. Fig. 3c shows a representation of the optical emission waveforms of Ar I for four pulse types. In all cases the emission

Table 1

Box Behnken analysis: Mass Spec and Coatings as related to reverse voltage parameters of delay (t_d), amplitude (U_r) and duration (t_r). Strongest dependencies are marked in bold, up arrows indicate a positive dependence.

	t_d	U_r	t_r	$t_d: U_r$	$t_d: t_r$	$U_r: t_r$	t_d^2	U_r^2	t_r^2
Ion flux ratios									
$\text{Si}^{1+}:\text{Ar}^{1+}$	-0.9 ▼	-0.40 ▼	-0.37 ▼	0.3			0.29	-0.13	-0.5
$\text{O}^{1+}:\text{O}_2^+$ flux	-0.5 ▼	-0.8 ▼	0.06	0.17			0.05	0.23	-0.81 ▼
$\text{Si}^{2+}:\text{Si}^{1+}$	-0.015 ▼	-0.016 ▼	0.024 ▲	-0.01			0.016	0.006	-0.031 ▼
Film properties									
Transmittance	-3.8 ▼	+1.5	-2.8 ▼	0.25		-0.8	-4.5		
Ra macroscopic	250 ▲	100	-120 ▼	100		90	-75		
Ra microscopic	-1.8 ▼	-1	2.8 ▲	-1.7		2.6 ▲	-1		

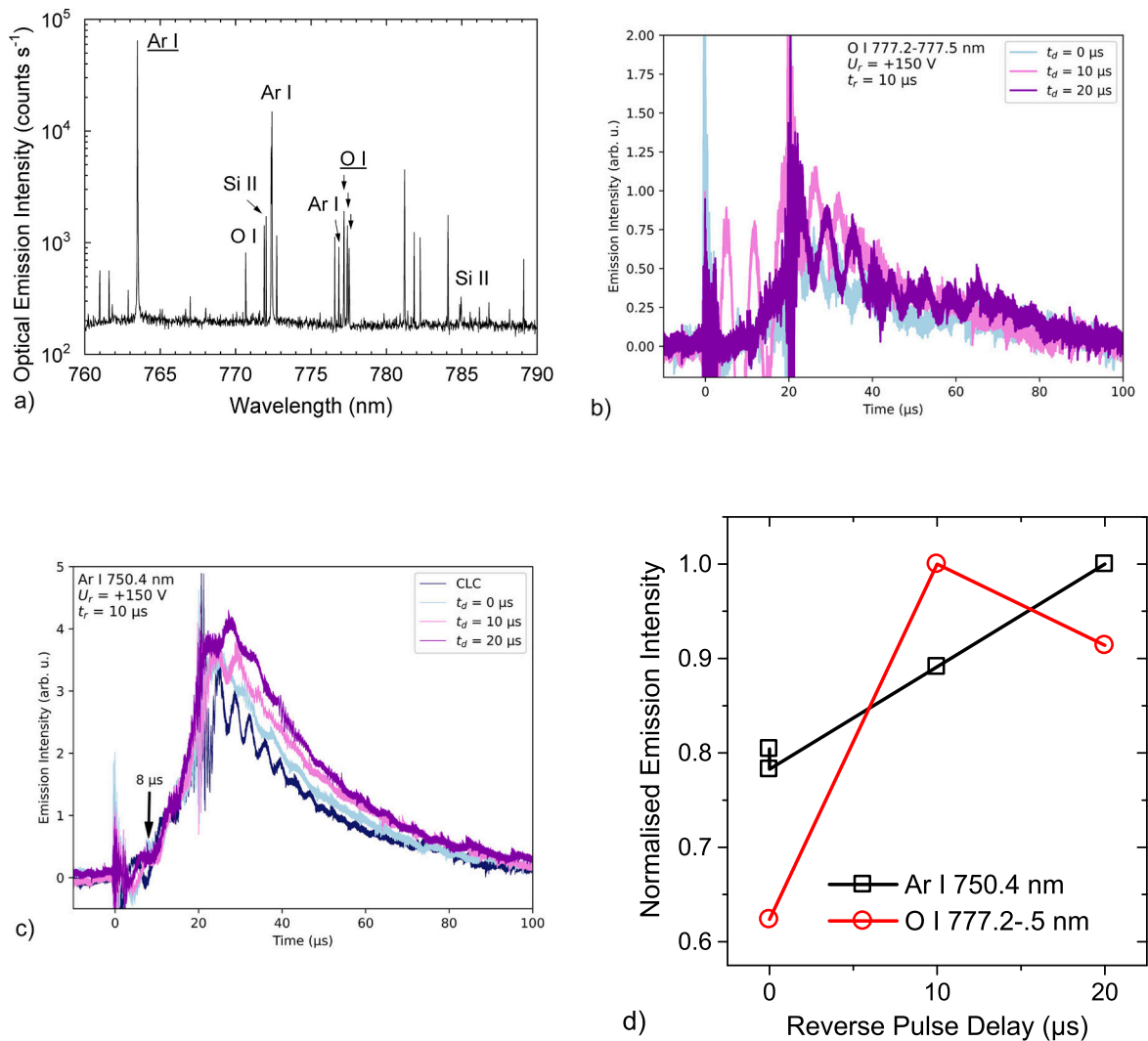


Fig. 3. a) Optical emission spectrum from reactive HIPIMS of Si in Ar and O₂ atmosphere. Underlined labels correspond to lines used for temporal evolution studies. b) Time evolution of O I emission contributions from 777.194, 777.4166 and 777.5388 nm for HIPIMS with reverse pulse with different delay times to applying the reverse voltage, c) Time evolution of Ar I emission at 750.387 nm for HIPIMS with reverse pulse with different delay times to applying the reverse voltage, and d) time-averaged emission intensity of Ar I and O I lines normalised to the maximum value of each line.

risers according to an exponential increase and falls according to an exponential decay. The CLC trace for Ar I in Fig. 3b and the traces for O I in Fig. 3c were of very low intensity, and exhibited oscillations, which were caused by the measurement circuit as detailed in Section 2.

Table 2 lists the decay times for O I and Ar I. The times are similar for both species and show little variation between modes. The decay times are a factor 10 higher than the ones reported for pulsed DC operation [11]. This could be attributed to the significant plasma density of the HIPIMS discharge compared to DCMS.

Significant variations in intensity are observed with reverse pulse

delay as shown in Fig. 3d. O I and Ar I emissions both increase by factor of 1.6 and 1.25 respectively at longer delays.

Important changes in the chemistry of the plasma are revealed through mass spectrometry measurements. Fig. 4 summarises the composition of ion fluxes to the substrate for the case of low reverse voltage applied without delay, low reverse voltage applied with delay, and high reverse voltage applied with delay of 10 μs. The relative fluxes of Si²⁺, Si¹⁺, Ar¹⁺, and Ar²⁺ are extracted from integrating the corresponding IEDFs. Significant differences are apparent depending on the pulse configuration. The configuration with low reverse voltage of U_r =

Table 2

Influence of reverse pulse delay times emission intensity decay times and integrated intensity for O I and Ar I compared to mid-frequency pulse DC magnetron sputtering [11].

t _d / U _r / t _r	Decay times (μs)		Integrated intensity (arb. u.)	
	Ar I 750 nm	O I 777 nm	Ar I 750 nm	O I 777 nm
0 / 120 / 2 × 1 (CLC)	21.2639 ± 0.0025		37	
0 / 150 / 10	22.0637 ± 0.0017	27.626 ± 0.016	36	
10 / 150 / 10	22.5877 ± 0.0017	22.762 ± 0.006	41	9.3
20 / 150 / 10	22.5311 ± 0.0019	40.39 ± 0.03	46	8.5
Pulsed DC	<2			

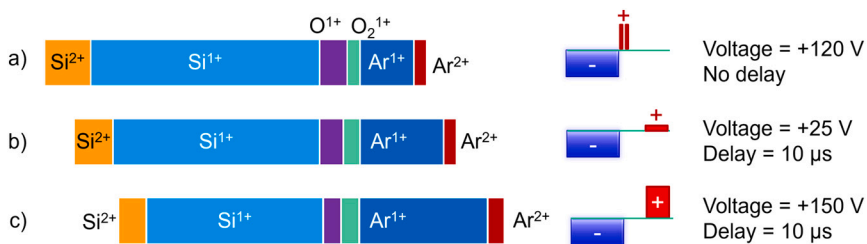


Fig. 4. Relative mass spectrometer count rates of Si and Ar ions arriving to a grounded substrate obtained from time-averaged energy-resolved mass spectrometry measurements for different reverse pulse configurations including a) $t_d = 0 \mu\text{s} / U_r = +120 \text{ V} / t_r = 2 \times 1 \mu\text{s}$ (CLC), b) $t_d = 10 \mu\text{s} / U_r = +25 \text{ V} / t_r = 10 \mu\text{s}$, and c) $t_d = 10 \mu\text{s} / U_r = +150 \text{ V} / t_r = 10 \mu\text{s}$.

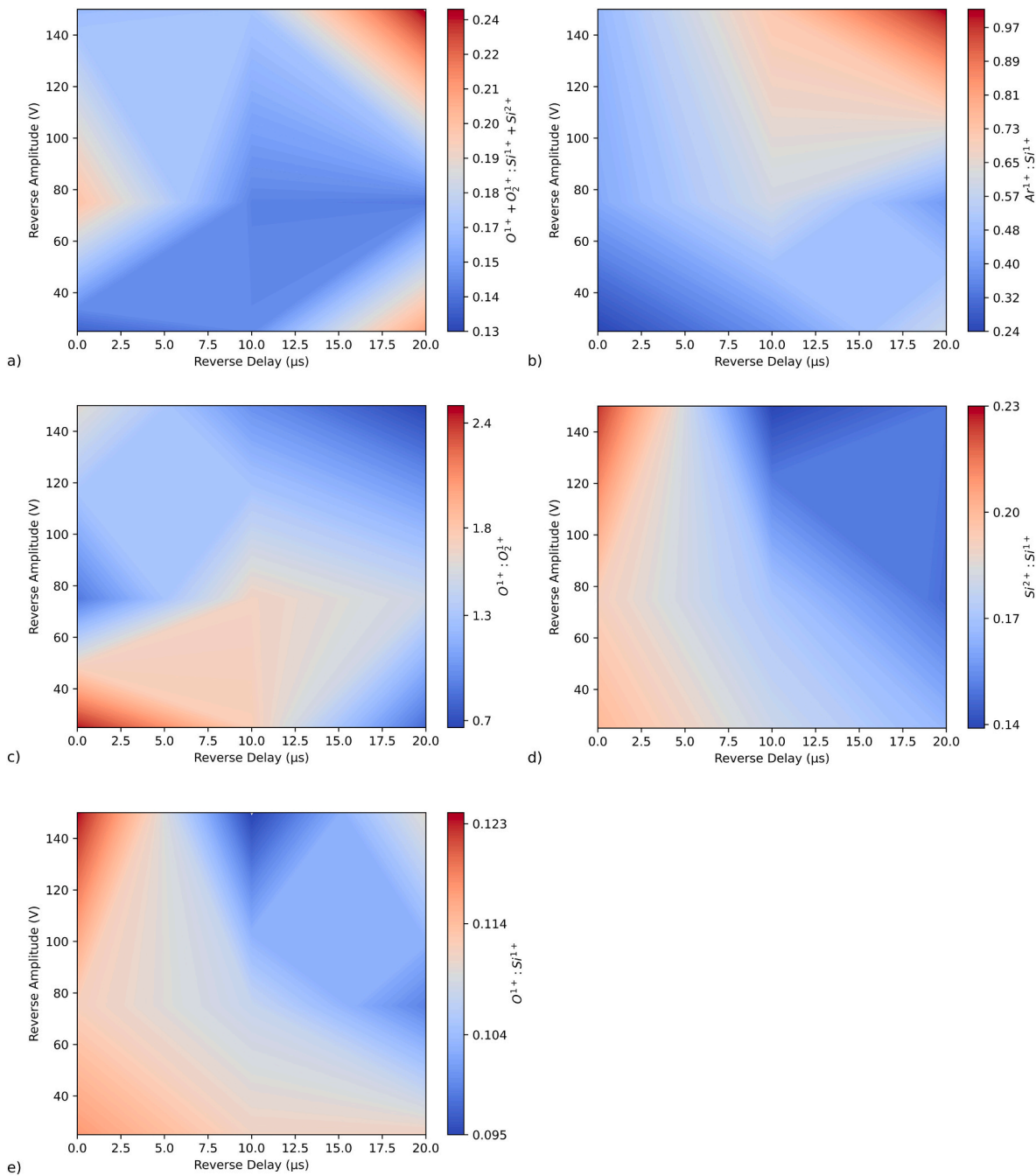


Fig. 5. Relative composition of ion fluxes arriving to a grounded substrate obtained from time-averaged energy-resolved mass spectrometry measurements for different reverse pulse configurations for a reverse pulse duration of 10 μs : a) Oxygen ions to Silicon ions ratio ($\text{O}^{1+} + \text{O}_2^{1+} : \text{Si}^{1+} + \text{Si}^{2+}$), b) Argon ion – to – Silicon ion ratio ($\text{Ar}^{1+} + \text{Ar}^{2+} : \text{Si}^{1+} + \text{Si}^{2+}$), c) Atomic Oxygen to molecular Oxygen ratio: ($\text{O}^{1+} : \text{O}_2^{1+}$), d) $\text{Si}^{2+} : \text{Si}^{1+}$ ratio, and e) Atomic Oxygen–to–Silicon ratio ($\text{O}^{1+} : \text{Si}^{1+}$).

+25 V applied with delay $t_d = 10 \mu\text{s}$ (Fig. 4b) presents a Si-rich plasma consistent with the high current densities on the target. These conditions approximate unipolar configuration as the reverse voltage is applied well beyond the complete decay of the discharge current and its amplitude is very low. The ratio between Si ($\text{Si}^{1+} + \text{Si}^{2+}$) and Ar ($\text{Ar}^{1+} + \text{Ar}^{2+}$) ions is intermediate compared to the CLC (Fig. 4a) and reverse circuit configurations (Fig. 4c). The highest Si^{1+} and Si^{2+} flux content (Fig. 4a) is observed when there is minimum delay in applying the reverse pulse, as is the case for the operation of the CLC circuit. The highest $\text{Ar}^{1+} + \text{Ar}^{2+}$ content is observed for long delay times of $t_d = 10 \mu\text{s}$ and high voltages of $U_r = +150 \text{ V}$ (Fig. 4c). These delay times are well beyond the complete decay of cathode current; therefore, the flux of gas ions is not a result of the reverse voltage accelerating ions away from the dense plasma region near the target. Moreover, the gas ion flux is in excess of that produced at the target when operating in unipolar mode. This indicates that gas ions are being produced as a result of the application of the reverse voltage in agreement with the OES analysis. In most cases, the O_2^+ fluxes follow the trend for Ar^{1+} , while O^{1+} are similar to Si. This indicates that O^{1+} may be predominantly produced in the dense plasma region near the target and can be accelerated towards the substrate if positive voltages are applied before the decay of discharge current. The majority of atomic oxygen ions come from dissociation of O_2 and a small fraction is sputtered from the target.

Fig. 5a shows the Oxygen-to-Silicon ion flux ratio for different reverse pulse durations and amplitudes. An increase of as much as factor of 1.8 is observed at high delays and high reverse voltages. An increase by a factor of 4 is also observed in the Argon-to-Silicon ions ratio as shown in Fig. 5b. In the parameter space investigated, the duration of the reverse pulse plays a more important role than its amplitude. The duration causes a factor of ~ 1.8 increase while for the amplitude the increase is by a factor of ~ 1.2 . The ratios changed on account of the absolute ion fluxes of gas and silicon ions changing in opposite directions, resulting in an overall increase in their ratio.

Fig. 5a and b shows that the delay and reverse voltage increase the fluxes of Oxygen and Argon relative to Si ions. Reversing the voltage results in a positive potential applied to the target, and converts it to an anode. The bulk plasma potential responds by rising a few volts above the voltage of said anode. The chamber walls, along with any floating surfaces, attain a negative potential with respect to the bulk plasma, converting them into cathodes and establishing a cathode sheath. The magnitude of the potential of the walls with respect to the bulk plasma is approximately equal to the reverse voltage amplitude plus $kT_e/2$. This negative potential attracts energetic particle bombardment to the wall surface, which accelerates electrons across the sheath and away from the grounded chamber walls and injects them into the bulk plasma producing additional gas ions near any grounded surfaces. The high-potential sheath created around the walls is also a barrier to electron losses and, together with the injection of electrons from the walls, induces electron heating in the plasma bulk [18]. Meanwhile the number of Silicon ions remains unchanged as they are produced during the negative voltage phase. The relative increase of the Oxygen and Argon fluxes against Si with reverse amplitude could be attributed to variations in total ionisation cross section of the species in the energy interval from 25 to 150 eV, where for molecular Oxygen it increases by a factor of 3.3, while for Si it reduces by a factor of 1.4. At low reverse voltages, the gas ion-Si ion ratio remains independent of delay due to the similar ionisation cross section for Si, Ar and O_2 at lower energy. As the energy is increased, the ionisation cross section for Si reduces while for O_2 and Ar it continues to increase [19,20]. Thus at high potentials and longer delay times, the gas species are ionised preferentially. The ionisation of both Ar and O_2 is most efficient at an electron energy of $\sim 100 \text{ eV}$, hence the maximum relative Oxygen ion and Argon ion fluxes are observed at reverse voltages of +150 V as shown clearly in Figs. 5a and 5b respectively.

At voltages above +25 V and delays of 10 μs , an intensive ionisation of gaseous species is observed.

In contrast, Fig. 5c shows that dissociation ratios of Oxygen ($\text{O}^{1+}:\text{O}_2^+$) is highest at low reverse voltages and minimum delays. The ratio is very strongly affected by the reverse pulse strategy and reduces by a factor of 3.7 when both U_r and t_d are high. In these conditions the bulk plasma is near the target surface and is still very dense, whereas the voltage is too low to cause intensive dissociation of O_2 . The prevalent effect is that of accelerating ions in the bulk plasma in the vicinity of the target towards the substrate. Since the bulk plasma is rich in dissociated Oxygen, its flux is maximised. As will be shown in the following section, the conditions for producing higher Oxygen dissociation levels coincide with the production of smoother films.

A similar effect is observed for the $\text{Si}^{2+}:\text{Si}^{1+}$ ratio (Fig. 5d), which reduces by a factor of 1.7 for long delays. At short delays the reverse voltage accelerates ions from the bulk plasma, which is rich in Si^{2+} ions, away from the target and towards the substrates. The higher the voltage, the higher the energy and greater the flux. At longer delays, the bulk plasma and the discharge current itself have already decayed, leaving small amounts of ions found in the bulk plasma, including Si^{1+} , Si^{2+} and O^{1+} , available for acceleration.

The atomic Oxygen-to-Silicon ion ratio is highest at highest reverse amplitude and shortest delay (Fig. 5e), similar to the $\text{Si}^{2+}:\text{Si}^{1+}$ ratio.

When the reverse voltage is applied immediately after the main pulse (delay is 0 μs), it appears in the presence of a high-density plasma near the target and chamber walls. The reverse fluxes to the target which neutralise surface charge are maximised, leading to the most efficient reduction in arcing probability. Additionally, any arcing events that occur in the off-times can be quenched rapidly, thereby minimising arc energy and damage to the films.

Conversely, when reverse is applied after the current has diminished, the governing effect is that of ionising the gaseous atmosphere. The additional ionisation of the gas environment may lead to activation of residual gas contaminants such as hydrogen, Oxygen and OH radicals whose density is highest near outgassing sources such as the walls and heaters, both of which are typically grounded. The intensity of outgassing is likely to be enhanced by bombardment of ions accelerated across the sheath which is established during the reverse pulse stage. In summary, these results clearly show that higher negative voltages may lead to enhanced electron energy and ion-induced degassing and cause a higher rate of incorporation of impurities in the film as discussed in the following section.

3.4. Thin film surface morphology

3.4.1. Macroscopic roughness

The macroscopic surface topology of the coatings was studied using optical microscopy. As shown in the optical micrographs in Fig. 6, the coatings exhibited wide variations in particle defect densities depending on the mode of applying the reverse voltage during deposition. In samples deposited with a 10 μs delay in reverse voltage, a significant proportion of the surface was covered with large macroparticle defects (Fig. 6a-c). The sample deposited using the CLC circuit and the samples deposited without delay in reverse voltage exhibited a more homogeneous surface as shown in Fig. 6d-h.

These observations tally well with the optical transmittance data (see Fig. 9 and pertaining discussion), with surfaces with larger defect coverage (Fig. 6a-c) exhibiting significant loss in transmittance compared to the smoother surfaces (Figs. 6d-h).

Although the surfaces of samples deposited at $t_d = 0 \mu\text{s}$, $U_r = +150 \text{ V} / t_r = 20 \mu\text{s}$, and $U_r = +25 \text{ V} / t_r = 20 \mu\text{s}$ shown in Fig. 6(g, h) appear rougher than those of samples deposited at $t_d = 0 \mu\text{s}$ with the CLC circuit ($U_r = +120 \text{ V}$, $t_r = 2 \times 1 \mu\text{s}$) and $U_r = +150 \text{ V} / t_r = 30 \mu\text{s}$ in Fig. 6(d-f), their microscopic roughness was up to a factor of 10 lower as detailed in the following section. At a setting of $t_d = 0 \mu\text{s} / U_r = +150 \text{ V} / t_r = 30 \mu\text{s}$, samples were deposited using two different arc detection thresholds of maximum current (I_{max}) – a standard level of 50 A (Fig. 6d) and a higher level of 100 A (Fig. 6e). Higher arc detection thresholds permit the

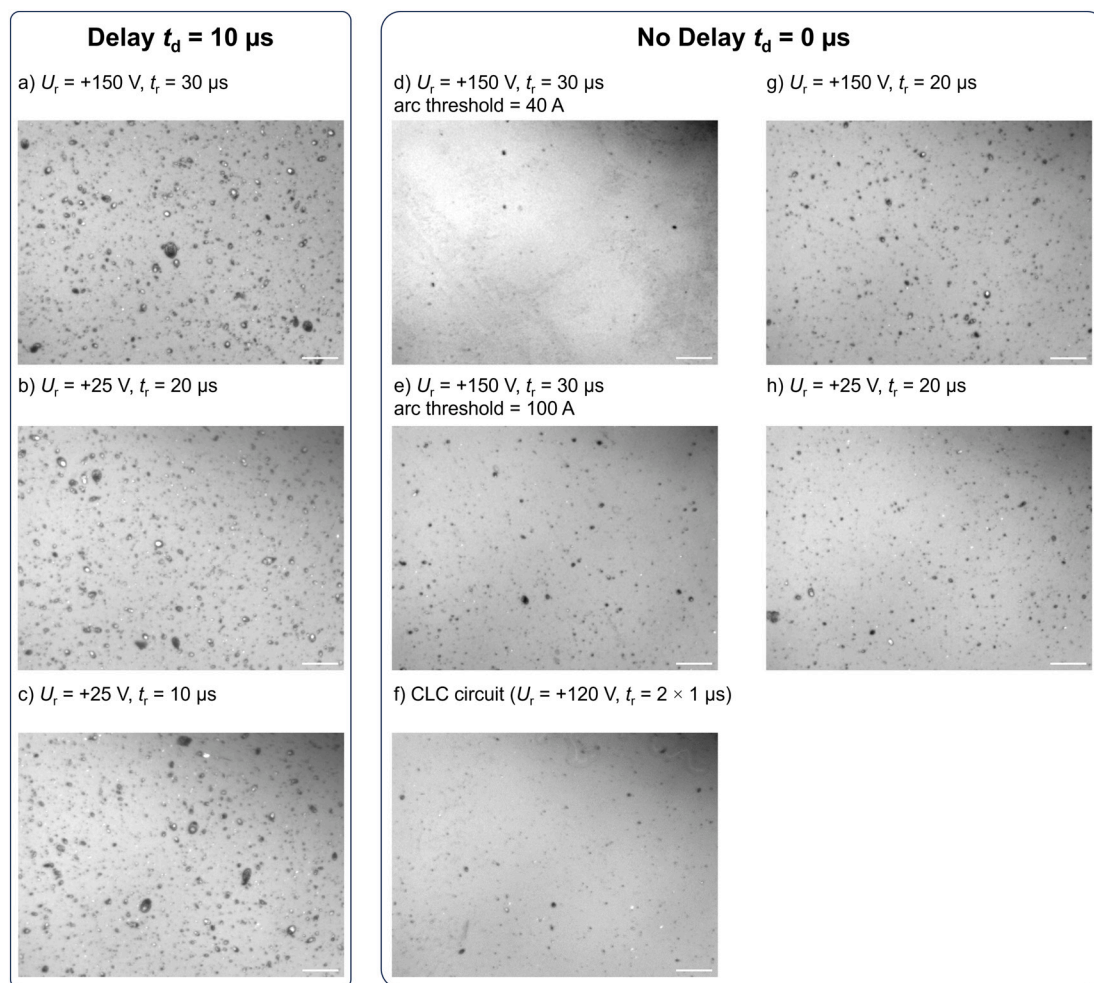


Fig. 6. Optical micrographs at a magnification of $100\times$ of the surface of coatings deposited with a delay in applying the reverse voltage of $t_d = 10 \mu\text{s}$ and a) $U_r = +150 \text{ V}$, $t_r = 30 \mu\text{s}$, b) $U_r = +25 \text{ V}$, $t_r = 20 \mu\text{s}$, and c) $U_r = +25 \text{ V}$, $t_r = 10 \mu\text{s}$, and no delay $t_d = 0 \mu\text{s}$ and d) $U_r = +150 \text{ V}$, $t_r = 30 \mu\text{s}$, e) $U_r = +150 \text{ V}$, $t_r = 30 \mu\text{s}$, f) CLC circuit ($U_r = +120 \text{ V}$, $t_r = 2 \times 1 \mu\text{s}$), g) $U_r = +150 \text{ V}$, $t_r = 20 \mu\text{s}$, and h) $U_r = +25 \text{ V}$, $t_r = 20 \mu\text{s}$. Scalebar = $50 \mu\text{m}$.

discharge to spend a longer time in an arc state, dissipate greater energy into the arc spot, produce more macroparticles and increase the roughness of the films. Roughness measurements shown in Fig. 8 confirm this observation.

3.4.2. Microscopic morphology

The microscopic features of the films were characterised by AFM on $1 \mu\text{m}^2$ and $400 \times 100 \text{ nm}$ areas as summarised in Fig. 7.

AFM scans of the morphology of the film surface revealed an amorphous material with a globular substructure. The globules were of diameter $\sim 50 \text{ nm}$ (Fig. 7a-d and g), except the sample deposited at $t_d = 0 \mu\text{s}$ / $U_r = +25 \text{ V}$ / $t_r = 20 \mu\text{s}$ where the globules were reduced to 20 nm (Fig. 7h). The reduction in globule size was accompanied with a reduction in Ra from 0.64 ± 0.03 to $0.29 \pm 0.04 \text{ nm}$ as demonstrated in Fig. 8 and Table 3. At a setting of $t_d = 0 \mu\text{s}$ / $U_r = +150 \text{ V}$ / $t_r = 30 \mu\text{s}$, samples were deposited using two different arc detection thresholds of maximum current – a standard level of $I_{\text{max}} = 50 \text{ A}$ (Fig. 7d) and a higher level of $I_{\text{max}} = 100 \text{ A}$ (Fig. 7e). The microscopic Ra values in both cases are similar. However, the macroscopic roughness was significantly increased for the higher threshold – see data point marked with an asterisk in Fig. 8.

In samples deposited with a $10 \mu\text{s}$ delay in reverse voltage, a significant proportion of the surface was covered with large macroparticle defects (Fig. 7a-c). The surface between the defects was exceptionally smooth, with Rmax reducing to 990 pm for $t_d = 10 \mu\text{s}$ / $U_r = +25 \text{ V}$ / $t_r =$

$20 \mu\text{s}$ (see detail scan in Fig. 7b). This could be attributed to the frequent arcing which produces relatively high content of Si ions with high energy and promotes the formation of a smooth surface. The samples deposited without delay in reverse voltage and high levels of reverse voltage of $+100$ to $+150 \text{ V}$ including the sample deposited using the CLC circuit, $t_d = 10 \mu\text{s}$ / $U_r = +25 \text{ V}$ / $t_r = 20 \mu\text{s}$ and $t_d = 10 \mu\text{s}$ / $U_r = +25 \text{ V}$ / $t_r = 20 \mu\text{s}$ exhibited very rough surfaces (Fig. 7d-f), with Ra reaching $1.6\text{--}18 \text{ nm}$ – a factor of 10 higher than the rest in the series. Deposition without delay in reverse voltage and low levels of U_r and/or t_r , including $t_d = 0 \mu\text{s}$ / $U_r = +25 \text{ V}$ / $t_r = 20 \mu\text{s}$ and $t_d = 0 \mu\text{s}$ / $U_r = +150 \text{ V}$ / $t_r = 20 \mu\text{s}$ resulted in smooth surfaces (Fig. 7g and h), low macroparticle density and some of the lowest roughness in the deposition parameter range (Fig. 8).

3.5. Transmission spectra

The light transmission characteristics of the films in the ultraviolet-to-visible spectral range are shown in Fig. 9. A major improvement in transmittance by ~ 10 percentage points is observed when removing the delay in applying the reverse voltage from $t_d = 10 \mu\text{s}$ to $0 \mu\text{s}$. The core determinant was found to be the incidence of arcing during deposition of the films and the prevalence of well-defined macro-defects on the surface as illustrated in Fig. 6. The highest arc damage was observed when the delay was $10 \mu\text{s}$, which was long compared to the decay of the current.

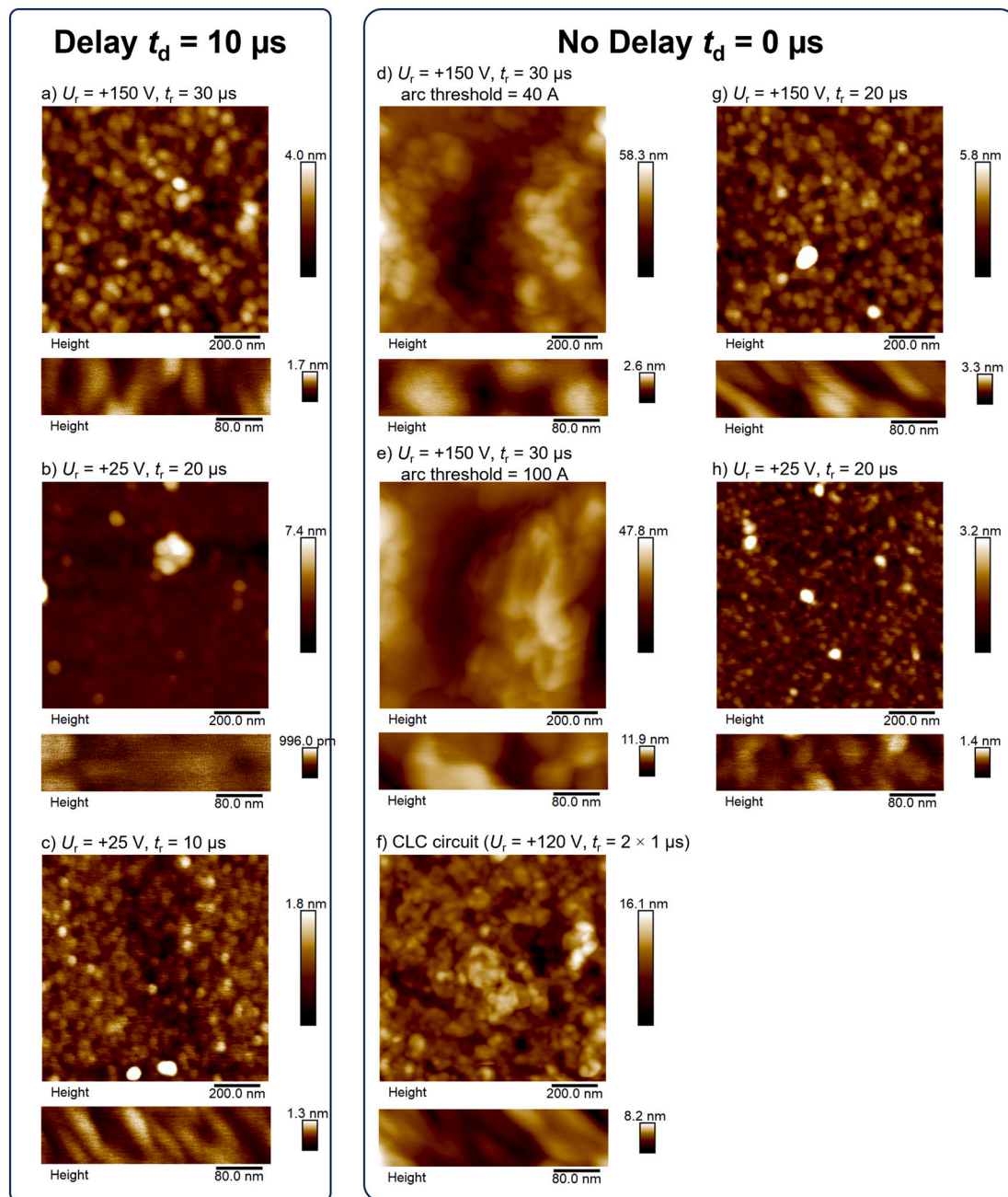


Fig. 7. AFM scans of the surface of SiO_x films deposited by HIPIMS with a delay in applying the reverse voltage of $t_d = 10 \mu\text{s}$ and a) $U_r = +150 \text{ V}$, $t_r = 30 \mu\text{s}$, b) $U_r = +25 \text{ V}$, $t_r = 20 \mu\text{s}$, and c) $U_r = +25 \text{ V}$, $t_r = 10 \mu\text{s}$, and no delay $t_d = 0 \mu\text{s}$ and d) $U_r = +150 \text{ V}$, $t_r = 30 \mu\text{s}$, e) $U_r = +150 \text{ V}$, $t_r = 30 \mu\text{s}$, f) CLC circuit ($U_r = +120 \text{ V}$, $t_r = 2 \times 1 \mu\text{s}$), g) $U_r = +150 \text{ V}$, $t_r = 20 \mu\text{s}$, and h) $U_r = +25 \text{ V}$, $t_r = 20 \mu\text{s}$.

3.6. Nano-hardness

The CLC reverse pulse strategy was selected for its ability to enhance metal ion flux to the substrates, reduce arcing probability, and lower macroscopic and microscopic roughness, whilst maintaining a high transparency of the films. The strategy based on HIPIMS and CLC allowed for a long operation of the cathode over 2.5 h and the deposition of a $1 \mu\text{m}$ thick layer within a stable process.

Fig. 10 shows the nano-hardness of films deposited using the CLC reverse pulse strategy benchmarked against other plasma-based deposition processes. The lowest hardness of approximately half of that of amorphous bulk substrate is observed for plasma-assisted chemical vapour deposited films (PACVD) due to the porous microstructure of the films [2]. Pulsed DC magnetron sputtering achieves approximately 90 %

of the bulk glass nano-hardness [5,15]. The HIPIMS-deposited films in this study achieve a nano-hardness of $10 \pm 1 \text{ GPa}$ and Young's modulus $77 \pm 9 \text{ GPa}$. This represents the highest nano-hardness amongst plasma deposition processes, even exceeding the hardness of bulk SiO_2 due to the high density of the microstructure. The film hardness is on par with that of microwave-deposited multilayer stacks of TiO_2 and SiO_2 [16].

4. Discussion

4.1. Plasma chemistry, arcing and process stability

The overall stability of the process was strongly influenced by the negative and positive pulse shape and timing of application of the reverse pulse. The process stability is influenced by the fact that the

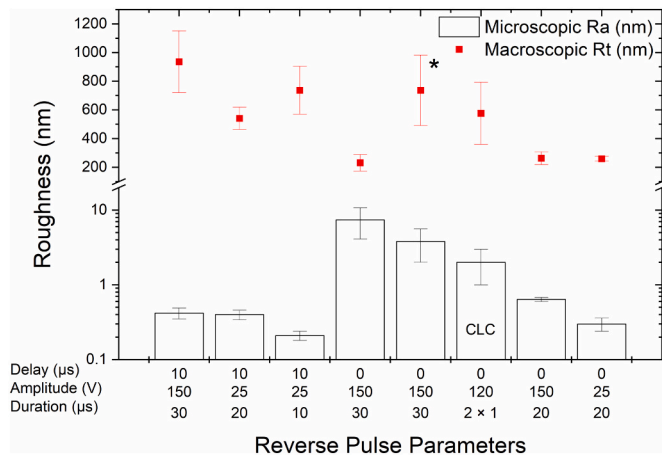


Fig. 8. Macroscopic roughness obtained from stylus profilometry, and microscopic roughness obtained from AFM images of smoothest areas between macroscopic defects. The asterisk marks deposition at higher than standard arc detection threshold, I_{max} .

discharge current is conducted through a multitude of asperities on the surface of the target. The sharp geometry of asperities enhances the electric field near their tip and increases the probability for field-enhanced electron emission. An asperity can conduct a certain amount of energy, before initiating field-enhanced thermoelectron emission, which causes it to overheat and triggers an avalanche reaction whereby more electrons are emitted causing heating and ultimately leading to a local explosion of the asperity and the transition of the discharge from glow to arc – so called arcing event. The threshold energy, given by the product of the critical current, j_{cr} , and critical (delay) time, t_{cr} , to explosion are related to the physical properties of the compound which is being sputtered from the surface including density (ρ), specific heat capacity (C_s), resistivity (ρ_e), temperature coefficient of resistivity (α), melting point of the material (T_c) and temperature at the start of the pulse (T_0) according to: [9,10].

$$j_{cr}^2 t_{cr} \leq \rho C_s \rho_e^{-1} \alpha^{-1} \ln(T_c/T_0) \quad (i)$$

During reactive sputtering of Silicon, the Silicon Dioxide compound that is formed on the surface of the target has orders of magnitude higher resistivity of 10^{14} – 10^{16} Ω -cm compared to 2.3×10^5 Ω -cm for Silicon. This severely reduces both j_{cr} and t_{cr} leading to a high probability of arcing even for low currents.

Additionally, arcing can occur when the dielectric compound is bombarded by ion flux from the plasma and accumulates a positive charge on its surface. Beyond a critical point, the dielectric formed by the compound is overwhelmed by the buildup of charge and breaks down, initiating an arcing event. Our experiments show that the shape of the current waveform plays an important role in determining the arcing probability. A rapid rise in the current led to arcing in practically every pulse. In contrast, a controlled gradual exponential increase in current is

beneficial in reducing the probability for glow-to-arc transition. Initially, the low-current stage ignites a low-density plasma which starts the sputtering of the target. The subsequent gradual increase in density ionises the sputtered flux taking it beyond the Ar gas ion flux whilst the dissociated Oxygen atom numbers increase relative to the molecular ones as shown in Fig. 4. The relatively short amount of time when the pulse current is at high level allows the current density to rise to as much as 0.5 Acm^{-2} without breaching the $j_{cr}^2 t_{cr}$ limit.

Another factor in reducing the arcing is the reverse (positive) voltage, which is intended to neutralise any charge that has built up during the pulse-on time when the plasma density is high, and compound formation occurs at the target surface as well as all surfaces in the

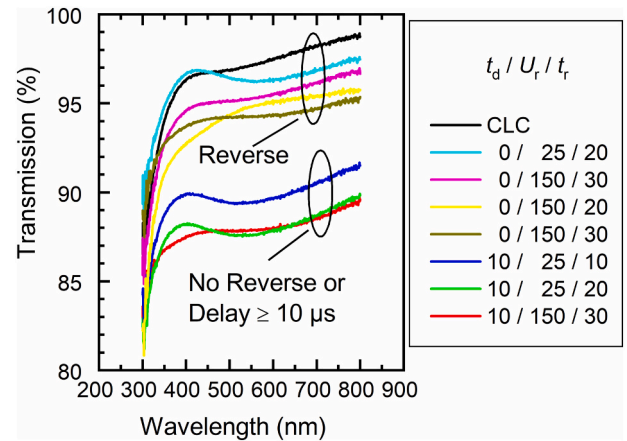


Fig. 9. Light transmission characteristics with respect to glass in the ultra-violet-to-visible spectral range.

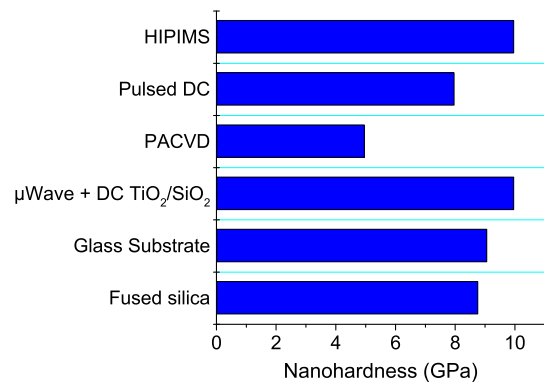


Fig. 10. Nanohardness of SiO_x films deposited by HIPIMS with CLC, pulsed DC magnetron sputtering [5,15], plasma-enhanced chemical vapour deposition (PACVD) [2], and microwave-assisted magnetron sputtering [16] in comparison to bulk SiO_2 glass and fused silica.

Table 3

Microscopic surface roughness (Rmax, Ra and Rq) determined from contact mode AFM scans, macroscopic surface profilometry (Rt) and transmittance at 550 nm of the samples as a function of reverse pulse configuration.

	t_d (μ s)	U_r (V)	t_r (μ s)	Rmax (nm)	Ra (nm)	Rq (nm)	Rt (nm)	Transmittance at 550 nm (%)
CLC	10	+150	30	4.9 ± 2.6	0.42 ± 0.07	0.52 ± 0.09	930 ± 210	87
	10	+25	20	8.9 ± 4.3	0.40 ± 0.06	0.69 ± 0.16	540 ± 80	87
	10	+25	10	4.4 ± 1.5	0.21 ± 0.03	0.33 ± 0.09	740 ± 170	89
	0	+150	30	68 ± 12	7.4 ± 3.3	9.5 ± 3.6	230 ± 60	94
	0	+150	30	33 ± 12	3.8 ± 1.8	4.8 ± 2.1	740 ± 240	96.5
	0	+120	2×1	20 ± 9.9	2.0 ± 1.0	2.7 ± 1.4	580 ± 210	97.5
	0	+150	20	10.5 ± 2.4	0.64 ± 0.04	0.91 ± 0.07	260 ± 50	95
	0	+25	20	5.2 ± 0.7	0.30 ± 0.06	0.46 ± 0.1	260 ± 18	97

chamber. The compound in the current experiments is a poor conductor so the surface cannot be neutralised by electrons flowing from the bulk of the target. Instead, a neutralising flux needs to be extracted from any residual plasma that is still present in the vicinity of the target surface. As the plasma current decays quickly, within 10 μs after voltage switch-off, the most efficient neutralisation occurs when the reverse voltage is applied as soon as possible after the end of the negative pulse and before the complete decay in current. The current experiments show that reverse pulsing without delay reduces arc damage more efficiently than when the delay extends beyond the decay time of the current, even if it is as low as 10 μs .

It was found that the arcing rate reported by the generator was similar in all depositions. However, it was realised that many arcs occurred just after the negative portion of the pulse was completed when the charge is still accumulated on the target, there is sufficient plasma density and the energy stored in the system, especially within long cables, is sufficient to initiate an arc and feed it for several tens of micro seconds, leading to coatings with more macroparticle defects. Arcing during pulse-off times is a major issue because the arc detection circuit is disabled and arcs are not detected. Crucially, they are not quenched, allowing them to run over several microseconds until a reverse voltage is applied.

Thus, for materials and processes that are prone to heavy arcing, it is recommended to use CLC or apply reverse voltage immediately after the process. This approach helps avoid arcs at the end of the pulse and minimises the energy of arcs occurring in the off-times, which might not be detected by the power supply. Using CLC or reverse voltage just after the pulse can result in better coating quality, such as reduced roughness, which improves optical transmission by dispersing less light. This is consistent with the coating analyses presented in Sections 3.4 and 3.5.

4.2. Plasma chemistry

The positive pulsing has a remarkable effect on plasma chemistry both near the substrates and near the target surface. The flux to the substrates and plasma emission near the target are strongly influenced by the timing of the reverse pulse relative to the decay of the plasma current and the magnitude of the reverse voltage.

When the reverse pulse is applied after the decay of the current pulse, i.e. with a significant delay after voltage switch-off, the relative flux of gas ions (Ar^{1+} and O_2^+) to the substrate increases along with the emission of Ar I and O I species. The enhanced optical emission indicates the presence of electrons with high energy sufficient to excite and ionise the gas near the target surface. The augmentation of the gas ion flux is most likely a result of gas ionisation near all the grounded walls and the grounded entrance orifice of the mass spectrometer.

The positive reverse voltage applied to the target increases the plasma potential of the bulk plasma to a level of a few volts above the applied voltage. The raised plasma potential creates a significant potential drop in the sheath around other electrodes, such as the grounded walls and grounded orifice of the spectrometer. The electrons accelerate across the sheath to an energy corresponding to the magnitude of the positive voltage; as the pressure is low, no energy losses due to collisions are expected in the sheath. These high-energy electrons are injected into the bulk plasma, thereby ionising the gas in the vicinity. The magnitude of the voltage plays a role in enhancing the ionisation probability per electron. For Ar, O and O_2 gas species, the highest ionisation cross section is near 100 eV, whereas for Si it is significantly lower at 30 eV. Increasing reverse voltage beyond 20 eV leads to more efficient gas ionisation and less efficient Si ionisation. As the plasma diagnostics results showed, reverse voltages beyond $U_r = +100$ V produce Ar gas ions as well as molecular oxygen O_2^+ thus lowering the Si ion to Ar ion ratio in the flux arriving to the substrates.

When the reverse voltage is applied without delay, it appears while there is still a significant density of plasma in the vicinity of the target surface before it has had a chance to decay. Initially, electrons respond

almost instantaneously at timescales of the order of 700 ps, creating a flux towards the target surface while the ions remain practically stationary (ion matrix sheath). The flux of electrons neutralises any positive charge buildup on the target and reduces the chances of arcing. As such, it is important to maximise the return electron flux by applying the reverse voltage without delay and before any significant decay in plasma has occurred.

The positive voltage also accelerates any target (Si) ions in the vicinity of the target away from it and towards the substrate. This process has longer characteristic times of several microseconds, therefore the length of the reverse pulse should be sufficient to allow for the slower reaction times of ions. The energetic target ion flux is detected at the mass spectrometer and substrate. Similarly, dissociated Oxygen is more abundant in the case of no delay than unipolar mode, as indicated by the increased ratio $\text{O}^{1+}:\text{O}_2^+$. O^{1+} is more likely to be found in the dense plasma region before current decay and is accelerated away from the target in a similar fashion to the target ions. When the delay in reverse voltage is longer than the current decay, there are very few particles in the vicinity of the target which can be accelerated away.

In summary, the magnitude of target and dissociated ions observed at the substrate is highest when the reverse voltage is applied without delay, lower in unipolar mode and lowest with delay and high level. Low amplitudes of the reverse voltage limit the production of gas ions and maximise the target-to-gas ion ratio. Optimum target discharging and reduced arc damage are obtained when the reverse voltage is applied without delay.

4.3. Grain morphology, surface roughness and optical transmittance

The grain morphology of the films is strongly affected by the plasma conditions and mode of applying the reverse voltage. When the reverse voltage is applied after the decay of the current pulse, there is insufficient discharging of the target surface which leads to a high incidence of energetic arcing events and a corresponding high density of macroparticle defects in the films (see Figs. 6a-c and 7a-c).

Even if applied without delay, the reverse voltage should be low enough to limit the production of excessive gas plasma at the chamber walls. Such plasma was observed to lead to arcing during the reverse voltage phase and even between pulses and result in a high defect density. Films deposited in such conditions develop a high roughness (Fig. 7a-c) on the microscopic scale. Larger-area AFM scans (not shown) reveal that the surface is comprised of a high density of sub-micron defects with a roughness of several tens of nanometres. This could be attributed to a high frequency of arcing and generation of large number of microscopic defects, which are embedded in the films. Additionally, high reverse voltages of $U_r = +150$ V and long duration of voltage reversal ($t_r = 30$ μs) may be responsible for ionising the gas environment near the chamber walls. Similar ionisation may be present when the CLC circuit is deployed, which reaches $U_r = +100$ V and, although short lived ($t_r = 5$ μs), it has a very strong effect because it appears when the decaying plasma density is still very high thus ensuring an intense burst of ionisation.

The walls are known to be a major reservoir of contaminants which outgas into the chamber. As such, the environment near the walls is likely to be highly contaminated, and by ionising it, the contaminants are activated and embedded in the film at high rates. This may result in contaminating particularly less prominent regions of the surface because they collect less deposition material. In contrast to the isotropic gaseous ion flux, the deposition flux is directional and is known to induce shadowing during growth. Contaminants restrict the surface diffusion of deposition material, so accumulating them at the grain boundaries reduces the influx of deposition material into those grain boundaries and stifles growth locally. Overall, this results in a high microscopic roughness as grain boundaries grow slower than the grain centre [6].

The smoothest films (Figs. 7h) are obtained when combining the benefits of a low or no delay $t_d = 0$ μs and low reverse voltage $U_r = +25$

V. The short delay ensures sufficiently high plasma density is available to push target ions towards the substrate and maintain high target-to-gas ion ratio as well as discharge the target and reduce arcing probability. The low voltage precludes the ionisation of the gas and activation of contaminants whilst still promoting the ionisation of Si, as well as enhancing acceleration away from the target in the direction of the substrate.

Raising the reverse voltage to $U_r = +150$ V at delay $t_d = 0$ μ s increases roughness by a factor of ~ 2 (Fig. 7g), and Ra values increase successively as reverse voltage duration is increased to $t_r = 20$ μ s (Fig. 7e) and $t_r = 30$ μ s (Fig. 7f) due to the overall density of ionised gases and contaminants being enhanced by the longer duration.

The best transparency is obtained when the arc damage is lowest and Si ion content is highest. The lowest arc damage is obtained when voltage reversal is immediate (delay of 0 μ s) and occurs in the early stages of decay of the current and before its complete vanishing. Under these conditions, the reverse voltage captures large amounts of electrons from the decaying plasma before they are able to diffuse outside the cathode sheath. Consequently, any charge buildup on the target surface is neutralised efficiently and arcing probability and arc energy are reduced.

Beyond arc damage, the transparency is improved with higher Si ion content relative to Ar ions due to lower mass of the Si ion and lower likelihood of inducing vacancy defects in the structure. This could account for both a better density and higher hardness of the films.

5. Conclusions

SiO₂ films were deposited using High Power Impulse Magnetron Sputtering with reverse voltage using a controlled current rise and a variety of strategies for applying a reverse (positive) voltage pulse following the main discharge pulse. The study explored the effects of amplitude, delay and duration of the positive pulse. An exponential current rise was found to minimise arcing and produce a stable reproducible process. Reverse voltage amplitudes of +75 V and beyond sustained an auxiliary plasma between the target, now playing a role of the anode, and the chamber walls and other grounded surfaces, as cathodes. The auxiliary plasma comprised process gases and is likely to ionise contaminants, the activation of which could explain the observed rough film surface due to a greater level of incorporation in the films, disruption of adatom mobility and promotion of globular grain morphology. Low reverse voltages of $\leq +25$ V had a positive effect on film microstructure, which could be attributed to an enhanced sputtered ion energy and the corresponding adatom mobility, resulting in low roughness and highly transparent films.

A key condition for achieving stable operation and obtaining high quality films was to minimise the delay in applying the reverse voltage so that it is shorter than the discharge current decay time constant. Meeting these conditions lower arcing probability by supplying sufficient electron flux to neutralise charge build-up on the target surface. Minimising the delay improves the quality of films by accelerating the maximum flux of target ions towards the substrates and lowering arc energy. High current density of 0.5 Acm⁻² and high Si:Ar and Si:O₂ ion ratios were achieved at low arc rates. The high ionisation ensured low microscopic roughness of Ra = 3 nm and high optical transmittivity. The films were of high density and exhibited a hardness of 10 GPa, similar to that of bulk silica and surpassing that of conventional thin film deposition technologies.

CRedit authorship contribution statement

A.W. Oniszczuk: Writing – review & editing, Methodology, Investigation. **D.S. Owen:** Writing – review & editing, Visualization, Methodology, Investigation. **D.A.L. Loch:** Writing – review & editing, Methodology, Investigation, Conceptualization. **P.Eh. Hovsepian:** Supervision, Funding acquisition, Conceptualization. **A.P. Ehiastian:**

Writing – review & editing, Writing – original draft, Visualization, Supervision, Resources, Project administration, Methodology, Investigation, Funding acquisition, Formal analysis, Data curation, Conceptualization.

Declaration of competing interest

The authors declare the following financial interests/personal relationships which may be considered as potential competing interests: At the time of writing, A.W.O. was employed by Trumpf Huettinger Sp. z o.o., Zielonka, Poland. At the time of writing, D.A.L.L. was employed by Trumpf Hüttinger GmbH + Co. KG, Freiburg, Germany.

Acknowledgements

A.P.E. and D.S.O. gratefully acknowledge the financial support of EPSRC grant EP/W009501/1. For the purpose of open access, the author has applied a Creative Commons Attribution (CC BY) licence to any Author Accepted Manuscript version arising from this submission. The authors would like to acknowledge the help of Dr. Sam Bort from Hiden Analytical Ltd. for valuable input in describing the sensitivity of the energy-resolved mass spectrometer for different mass/charge ratios.

Data availability

The data that support the findings of this study are available from the corresponding author upon reasonable request.

References

- [1] V. Sittinger, O. Lenck, M. Vergöhl, B. Szyszka, G. Bräuer, Applications of HIPIMS metal oxides, *Thin Solid Films* 548 (2013) 18–26.
- [2] K. Taeschner, H. Bartzsch, P. Frach, E. Schultheiss, Scratch resistant optical coatings on polymers by magnetron-plasma-enhanced chemical vapor deposition, *Thin Solid Films* 520 (2012) 4150–4154.
- [3] J. Huang, J. Mu, Y. Cho, C. Winter, V. Wang, Z. Zhang, K. Wang, C. Kim, A. Yadav, K. Wong, S. Nemani, E. Yieh, A. Kummel, Low-kSiOx/AlOx nanolaminate dielectric on dielectric achieved by hybrid pulsed chemical vapor deposition, *ACS Appl. Mater. Interfaces* 15 (2023) 56556–56566.
- [4] A. Macleod, Chapter 12 - optical thin films, in: Anonymous, Elsevier Inc, 2018, pp. 379–416.
- [5] O. Zywitzki, H. Sahn, M. Krug, H. Morgner, M. Neumann, Comparison of structure and properties of SiOx coatings deposited by reactive pulsed magnetron sputtering (PMS) and by hollow cathode activated EB evaporation (HAD), *Surf. Coat. Technol.* 133–134 (2000) 555–560.
- [6] P.B. Barna, M. Adamik, Fundamental structure forming phenomena of polycrystalline films and the structure zone models, *Thin Solid Films* 317 (1998) 27–33.
- [7] P.E. Hovsepian, A.P. Ehiastian, Six strategies to produce application tailored nanoscale multilayer structured PVD coatings by conventional and High Power Impulse Magnetron Sputtering (HIPIMS), *Thin Solid Films* 688 (2019) 137409.
- [8] A.P. Ehiastian, A. Vetushka, Y.A. Gonzalvo, G. Safran, L. Szekeley, P.B. Barna, Influence of high power impulse magnetron sputtering plasma ionization on the microstructure of TiN thin films, *J. Appl. Phys.* 109 (2011) 104314.
- [9] E.A. Litvinov, G.A. Mesyats, D.I. Proskurovskii, Field emission and explosive electron emission processes in vacuum discharges, *Soviet physics.Uspekhi.* 26 (1983) 138–159.
- [10] G.A. Mesyats, D.I. Proskurovsky, *Pulsed Electrical Discharge in Vacuum*, Springer-Verlag, Berlin; New York, 1989.
- [11] A. Belkind, W. Zhu, J. Lopez, K. Becker, Time-resolved optical emission spectroscopy during pulsed dc magnetron sputter deposition of Ti and TiO₂ thin films, *Plasma Sources Sci. Technol.* 15 (2006) S17–S25.
- [12] K.A. Reck, Y. Bulut, Z. Xu, S. Liang, T. Strunskus, B. Sochor, H. Gerdes, R. Bandorf, P. Müller-Buschbaum, S.V. Roth, A. Vahl, F. Faupel, Early-stage silver growth during sputter deposition on SiO₂ and polystyrene – comparison of biased DC magnetron sputtering, high-power impulse magnetron sputtering (HIPIMS) and bipolar HIPIMS, *Appl. Surf. Sci.* 666 (2024) 160392.
- [13] M.A. Law, F.L. Estrin, P.M. Bryant, M.D. Bowden, J.W. Bradley, Evidence for fireballs in bipolar HiPIMS plasmas, *Plasma Sources Sci. Technol.* 32 (2023) 025015.
- [14] R. Hippler, M. Cada, Z. Hubicka, Time-resolved diagnostics of a bipolar HiPIMS discharge, *J. Appl. Phys.* 127 (2020) 203303.
- [15] S. Bruns, S. Montzka, W. Reimann, M. Vergöhl, Comparison of abrasive tests for transparent optical coatings, *Thin Solid Films* 532 (2013) 73–78.
- [16] M. Mazur, D. Wojcieszak, D. Kaczmarek, J. Domaradzki, S. Song, D. Gibson, F. Placido, P. Mazur, M. Kalisz, A. Poniedzialek, Functional photocatalytically

- active and scratch resistant antireflective coating based on TiO₂ and SiO₂, *Appl. Surf. Sci.* **380** (2016) 165–171.
- [17] F. Walk, R. Valizadeh, J.W. Bradley, Ion energy analysis of a bipolar HiPIMS discharge using a retarding field energy analyser, *Plasma Sources Sci. Technol.* **31** (2022) 065002, <https://doi.org/10.1088/1361-6595/ac6a0d>.
- [18] E.V. Barnat, G.R. Laity, S.D. Baalrud, Response of the plasma to the size of an anode electrode biased near the plasma potential, *Phys. Plasmas* **21** (10) (1 October 2014) 103512, <https://doi.org/10.1063/1.4897927>.
- [19] Y.-K. Kim, K.K. Irikura, M.E. Rudd, M.A. Ali, P.M. Stone, J. Chang, J.S. Coursey, R. A. Dragoset, A.R. Kishore, K.J. Olsen, A.M. Sansonetti, G.G. Wiersma, D.S. Zucker, M.A. Zucker, NIST Standard Reference Database 107, 2004, <https://doi.org/10.18434/T4KK5C>.
- [20] S.D. Loch, C.J. Favreau, M.S. Pindzola, Electron-impact ionization of the Si atom, *J. Phys. B Atomic Mol. Phys.* **52** (2019) 055205.